

Plasmon Localization and Giant Fields in an Open-Resonator Metasurface for Surface-Enhanced-Raman-Scattering Sensors

Andrey K. Sarychev^{1,*}, Andrey Ivanov¹, Andrey N. Lagarkov,¹ Ilya Ryzhikov,¹ Konstantin Afanasev,¹ Igor Bykov,^{1,2} Grégoire Barbillon³, Nikita Bakholdin⁴, Mikhail Mikhailov,⁴ Alexander Smyk,⁵ Alexander Shurygin⁵, and Alexander Shalygin⁶

¹ Institute for Theoretical and Applied Electrodynamics, Russian Academy of Sciences, Moscow 125412, Russia

² Laboratory of Nano-Bioengineering, National Research Nuclear University MEPhI (Moscow Engineering Physics Institute), 31 Kashirskoe shosse, Moscow 115521, Russia

³ EPF-Ecole d'Ingénieurs, 55 Avenue du Président Wilson, Cachan 94230, France

⁴ National Research University “Moscow Power Engineering Institute”, Krasnokazarmennaya 14, Moscow 111250, Russia

⁵ James River Branch llc, 8, Tvardovsky st., Strogino Industrial Park, Moscow 123458, Russia

⁶ Lomonosov Moscow State University, Faculty of Physics, GSP-1, 1-2 Leninskiye Gory, Moscow 119991, Russia

(Received 29 October 2021; revised 14 March 2022; accepted 16 March 2022; published 15 April 2022)

We present metal-dielectric metasurfaces fabricated from metal periodical nanograting deposited on a dielectric substrate. The metasurface consists of a modulated dielectric, which is covered by a thin silver layer. The metasurface operates as an open plasmon resonator. The theory of plasmons excited in the open resonator formed by a metal nanograting is presented. The large local electromagnetic field is predicted for optical frequencies. The excitation of plasmons is experimentally demonstrated in the metasurface designed on a 4-in. Si wafer. The enhancement of the local electric field results in surface-enhanced Raman scattering (SERS). To investigate the SERS effect, the metasurface is covered with a thin layer of the 4-mercaptophenylboronic acid that molecules form covalent bonds with the silver nanolayer. The enhancement of the Raman scattering serves as a proof of concept. We obtain a detection limit of 230 nM for molecules of 4-mercaptophenylboronic acid.

DOI: 10.1103/PhysRevApplied.17.044029

I. INTRODUCTION

The design of a nanoresonator with a high enhancement of the local electric field is an important point for the application to the surface-enhanced Raman scattering (SERS) and other plasmon-enhanced spectroscopies. It is useful to increase the selectivity and sensitivity of biological and chemical sensing [1–4]. A couple of fabrication techniques allow the production of sophisticated resonant substrates with the controllable shape and arrangement of the resonators [5]. These techniques include focused ion-beam lithography [6], electron-beam lithography [7–10], x ray, UV, plasmonic cavity lens and interference lithography [11–16], nanoimprint lithography [17–19], nanosphere lithography [20–23], laser-induced transfer metal nanodroplets [24]. Some of them allow realizing reproducible SERS substrates with a lower cost and a larger active surface area, for example, interference lithography. In Refs. [11,15], the gold and hybrid gold-silver nanodisk array fabricated via x-ray interference

lithography is proposed. The effectiveness of the structures has been proven by the detection of a low concentration of Rhodamine 6G (R6G) molecules via SERS with enhancement factor $10^5 - 10^6$. The authors admitted high sensitivity, reproducibility, and stability of such structures. In Ref. [16], silver nanohole arrays are proposed. A photoresist layer sandwiched with two Ag layers increases the Q factor of nanoresonators and the sensitivity. The SERS substrates exhibited enhancement factors G of 10^7 that are capable of monolayer detection of R6G molecules. It should be noted that optically mirror underlayer, which is designed to increase Q factor, was theoretically predicted and experimentally investigated by the authors [4,25–27]. Theoretical predictions and experimental studies show giant electromagnetic field fluctuations in the case of almost touched plasmonic nanoparticles [2,28–36]. It is shown that plasmonic nanocavities confining the light to unprecedently small volumes support multiple types of modes. In Refs. [37–39], the spectra of plasmon oscillations occurring in a dimer of two closely set nanospheres or nanoellipsoids are found in the quasistatic approximation. The respective analytical expressions are obtained in the

* sarychev_andrey@yahoo.com

form of infinite series of special functions. The amplification by many orders on the magnitude of the spontaneous emission is predicted for an atom placed in between silicon carbide (SiC) nanoballs. The different nature of the interparticle modes leads to the mode beating within the nanocavity and the Rabi oscillations, which alters the spatiotemporal dynamics of the hybrid system [40]. By intermixing plasmonic excitation in nanoparticle arrays with excitons in a WS_2 monolayer inside a resonant metal microcavity, the hierarchical system was fabricated with the collective microcavity-plasmon-exciton Rabi splitting exceeding 0.5 eV at room temperature. Gap-surface plasmon metasurfaces, which consist of a subwavelength thin dielectric spacer sandwiched between an optically thick film of metal and arrays of metal subwavelength elements arranged in a strictly or quasiperiodic fashion, have a possibility to fully control the amplitude, phase, and polarization of the reflected light [30,41]. Open resonators can very effectively accumulate the electromagnetic energy (see Ref. [42]). In the optical frequency range, a corrugated metal surface can operate as an open resonator and generate a large local electric field [43–46]. The method of the transformation optics was developed to calculate optical properties of metamaterials [47,48]. This method was used to investigate reflection from the metal gratings in recent Refs. [49–52]. The authors have developed an original conformal mapping that transforms one-side metal grating into a rectangular metal slab that optical properties can be found. For instance, to calculate the reflection of an electromagnetic wave, the metal grating is replaced by a thin plane metal film. The developed method was used to theoretically investigate broadband THz absorption in graphene metasurfaces [53], optical properties of singular metal surfaces [51,54,55], nonlocal effects [56], and calculating of the energy loss of an electron flying over the metal modulation [57]. Strong motivation for the investigation of open plasmon resonators is the SERS effect, which is mainly due to the local electric field enhancement. The SERS effect enables identification of trace molecules captured by the corrugated metal surface. The SERS is extremely helpful for medical diagnostics, for instance, for cancer detection, imaging, and therapy, and it is used for drug delivery, quantitative control of biomarkers, including glycated proteins and cardiovascular biomarkers [58–63].

In this paper, we present the analytical theory as well as experimental observation of the plasmons excited in open resonators formed by a periodic metal grating. The model metal film, which mimics the films obtained in our experiments, is solved by conformal mapping. The mapping converts a modulated film into the cylinder while the incident electromagnetic wave converts into the magnetic monopole that excites the cylinder. Note that our mapping of the film and the presentation of the incident wave are different from that of Refs. [49,50]. Our

method allows the resonance conditions to be analytically obtained when it is possible to achieve the largest electromagnetic field enhancement both inside and in the vicinity of the plasmonic grating. This will increase the sensitivity of SERS probing and other surface-enhanced spectroscopies. The electromagnetic field distribution in the three-dimensional open plasmon resonators are also discussed. The modulated silver film is produced by a four-ray holographic process and its optical properties are measured. The silver metasurfaces are covered by molecules of 4-mercaptophenylboronic acid to investigate the SERS in metasurfaces made by optical interference lithography. SERS substrates are easy made and low cost for mass production, and they have allowed achieving a detection limit of 230 nM for molecules of 4-mercaptophenylboronic acid (4-mPBA). The smooth spatial structure of the film is convenient for the analyte deposition and can be tuned for effective adsorbing and sensing microscopic objects like protein molecules or viruses [63,64].

II. ANALYTICAL THEORY AND COMPUTER SIMULATIONS

We consider periodic metal gratings that support localized plasmons whose size can reach a few hundred nanometers. The metal gratings with two-side modulation efficiently concentrate and store electromagnetic energy. The local electric field is resonantly enhanced. The localized plasmons are analytically calculated using a quasistatic approximation for the nanogratings whose dimensions (thickness and modulation) are much smaller than the wavelength λ . Full-scale computer simulations of two- and three-dimensional metal grating are also presented.

A. Plasmon resonance in metal nanotube

To understand how the metasurface works, let us solve a simple two-dimensional plasmonic system, which is interesting by itself, since it has a nontrivial analytical solution. We investigate the plasmon resonance and the corresponding electromagnetic field enhancement in the metal nanotube that radius and thickness are much smaller than the wavelength λ . The length of the metal nanotube is much larger than the radius. The vector of the external electric field lies in u - v plane perpendicular to the tube axis. Since the transversal dimensions of the nanotube is much smaller than the wavelength the problem is reduced to the two-dimensional problem of the excitation of the infinite metal nanotube by the $E = \{E_u, E_v\}$ electric field, which is normal to the tube axis. For further simplification, we neglect retardation effects and use the quasistatic approximation when the plasmonic electric field is found from the electric potential $\varphi(u, v)$. The two-dimensional problem can be solved by considering the potential, electric field, and charge in u - v plane using the theory of functions

of a complex variable. All the distances are measured in terms of the internal radius of the nanotube.

Thus, we calculate the plasmon resonance and the field enhancement in a metal ring with radius r_0 , the thickness d_0 , and the metal permittivity ϵ_m , shown in Fig. 1 by red color. To find the field in the ring, we introduce the Descartes coordinates u , v , and the complex variable $w = u + iv$. The ring has the center at $u = v = 0$. It is surrounded by a dielectric host ϵ_d , blue color in Fig. 1; the medium inside the ring has permittivity ϵ_1 (light green in Fig. 1). The electromagnetic field is excited by the point “magnetic” monopole, which generates in the surrounding space the electric potential $\varphi_s = \text{Re}\varphi_{\text{sing}}$, where the complex potential φ_{sing} equals to

$$\varphi_{\text{sing}} = iE_0 \ln(w - x_0), \quad (1)$$

where $u = x_0$ and $v = 0$ are coordinates of the monopole (black dot and horizontal blue line in Fig. 1). The exact nature of the monopole is irrelevant for the material presented below. The monopole oscillates with the frequency ω , and the amplitude E_0 is assumed, for simplicity, to be positive $E_0 > 0$. Recall the quasistatic approximation is used, when the field retardation is neglected. Then, the electric potential φ is the solution of the Laplace equation $\Delta\varphi = 0$ that holds in all the space but the monopole center. As usual in a two-dimensional (2D) problem, a complex electric field is introduced $\tilde{E} = E_u - iE_v = -d\varphi/dw$. The field is expanded into radial $E_r = \text{Re}(w\tilde{E})/r \equiv (E_u u + E_v v)/r$ and angular $E_\phi = -\text{Im}(w\tilde{E})/r \equiv (-E_u v + E_v u)/r$ components, where $r = |w| = \sqrt{u^2 + v^2}$. The electric

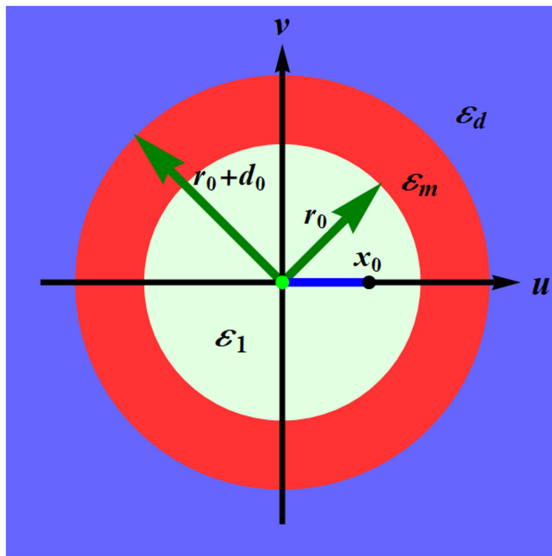


FIG. 1. Metal ring in the u - v plane; permittivity of internal space ϵ_1 , metal permittivity ϵ_m , permittivity of outer space ϵ_d , and a “magnetic” monopole placed at $u = x_0, v = 0$.

charges, induced by the monopole, are uniformly distributed in the metal ring when the monopole is placed in the center. Therefore, the angular component of the electric field remains to be the same inside and outside the ring. For the central monopole ($x_0 = 0$) with amplitude $E_0 > 0$, the interior electric field $E^{(i)}(r < 1)$, the field $E^{(m)}(1 \leq r \leq 1 + d_0)$ in the ring, and the outer field $E^{(e)}(r > 1 + d_0)$ have only angular components. The interior, ring, and outer fields are all equal to $E_r^{(i)} = E_r^{(m)} = E_r^{(e)} = 0$ and $E_\phi^{(i)} = E_\phi^{(m)} = E_\phi^{(e)} = E_0/r$. As we see, the central monopole does not excite a plasmon regardless of the value of the metal permittivity ϵ_m . Yet, this is an unstable solution. Plasmons are excited when the monopole is shifted from the center. Suppose that the monopole is set at $u = x_0 < 1, v = 0$. The interior complex potential is equal to

$$\begin{aligned} \varphi^{(i)}(w) &= \varphi_{\text{sing}}(w) + iE_0\varphi_{\text{reg}}^{(i)}(w), \\ &= iE_0[\ln(w - x_0) + \varphi_{\text{reg}}^{(i)}(w)], \quad r \leq 1, \end{aligned} \quad (2)$$

where $\varphi_{\text{reg}}^{(i)}(w)$ is a regular part of the interior potential that can be expressed in series in positive powers of w . To further simplify the consideration, we neglect for a moment the loss in the metal assuming that permittivity ϵ_m has zero imaginary part. The complex interior field is equal to

$$\begin{aligned} \tilde{E}^{(i)}(w) &= -\frac{d\varphi(w)}{dw} = -iE_0 \left[\frac{1}{w - x_0} + \sum_{n=1}^{\infty} A_n w^{n-1} x_0^n \right], \\ &\quad r \leq 1, \end{aligned} \quad (3)$$

where $0 < x_0 < 1$ and it is still assumed that E_0 is real. The first term in Eq. (3) is expanded in series of $(x_0/w)^n$ for $x_0 < |w| < 1$, and we obtain

$$\begin{aligned} \tilde{E}^{(i)}(w) &= -iE_0 \left[w^{-1} + \sum_{n=1}^{\infty} x_0^n (A_n w^{n-1} + w^{-n-1}) \right], \\ &\quad r \leq 1, \end{aligned} \quad (4)$$

where coefficients A_n take real values. The electric field in the metal ring is expanded in the Laurent series:

$$\begin{aligned} \tilde{E}^{(m)}(w) &= -iE_0 \left[w^{-1} + \sum_{n=1}^{\infty} x_0^n (B_n w^{-n-1} + C_n w^{n-1}) \right], \\ &\quad 1 < r < 1 + d, \end{aligned} \quad (5)$$

and the outer complex field decreases when the radius $r \equiv |w|$ goes to infinity:

$$\begin{aligned} \tilde{E}^{(e)}(w) &= -iE_0 \left[w^{-1} + \sum_{n=1}^{\infty} x_0^n D_n w^{-n-1} \right], \\ &\quad r \geq 1 + d. \end{aligned} \quad (6)$$

These complex fields can be split in radial and angular parts, namely,

$$E = \{E_r, E_\phi\} = \left\{ \operatorname{Re} \left[\tilde{E} \frac{w}{r} \right], -\operatorname{Im} \left[\tilde{E} \frac{w}{r} \right] \right\}.$$

For example, the internal field $E^{(i)}$ has the following radial and angular components:

$$\begin{aligned} \{E_r^{(i)}, E_\phi^{(i)}\} &= E_0 \{0, r^{-1}\} + E_0 \sum_{n=1}^{\infty} r^{-n-1} x_0^n \{(A_n r^{2n} - 1) \\ &\quad \times \sin(n\phi), (A_n r^{2n} + 1) \cos(n\phi)\}, \quad x_0 < r \leq 1. \end{aligned} \quad (7)$$

This $\{E_r, E_\phi\}$ expansion of the internal $E^{(i)}$, ring $E^{(m)}$, and outer $E^{(e)}$ fields holds even if the coefficients A_n, B_n, C_n, D_n are complex values. The coefficients ascribe complex values since the metal permittivity has imaginary part $\varepsilon_m = \varepsilon_{m1} + i\varepsilon_{m2}$ due to Ohmic loss.

The value of the intensity $I^{(i)} = |E^{(i)}|^2 / |E_0|^2$ of the internal field, which is averaged over the internal surface of the metal ring, ($|w| \equiv r = 1$) is equal to

$$\begin{aligned} \langle I^{(i)} \rangle &= \frac{1}{2\pi} \int_0^{2\pi} |E^{(i)}(r=1, \phi)|^2 d\phi \\ &= 1 + \frac{1}{2} \sum_{n=1}^{\infty} x_0^{2n} (|A_n|^2 + 1) \equiv 1 + \sum_{n=1}^{\infty} I_n, \end{aligned} \quad (8)$$

where the coefficients A_n are given below by Eq. (12). The coefficients A_n, B_n, C_n, D_n in Eqs. (3)–(8) are found from the boundary conditions for the electric fields at internal surface ($|w| = 1$) and outer surface ($|w| = 1 + d_0$) of the ring:

$$\varepsilon_1 E_r^{(i)} = \varepsilon_m E_r^{(m)}, \quad E_\phi^{(i)} = E_\phi^{(m)}, \quad |w| = 1, \quad (9)$$

$$\varepsilon_m E_r^{(m)} = \varepsilon_d E_r^{(e)}, \quad E_\phi^{(m)} = E_\phi^{(e)}, \quad |w| = 1 + d_0, \quad (10)$$

where ε_1 , ε_m , and ε_d are the permittivities of the internal space ($r \leq 1$), metal ring ($1 < r < 1 + d_0$), and the outer space ($r \geq 1 + d_0$), respectively. We substitute the series (3)–(7) in the above boundary equations and equate the coefficients at the same power of x_0 . It is easy to verify that the coefficients at x_0^n in all series (3)–(7) have the same angular dependence. Thus, the following basic equations are obtained:

$$\begin{aligned} A_n + 1 &= B_n + C_n, \quad \varepsilon_1 (A_n - 1) = \varepsilon_m (C_n - B_n), \\ B_n + C_n d_{2n} &= D_n, \quad \varepsilon_m (B_n - C_n d_{2n}) = \varepsilon_d D_n, \end{aligned} \quad (11)$$

where $d_{2n} = (1 + d_0)^{2n}$. Solution of these equations gives the coefficients

$$\begin{aligned} A_n &= \frac{d_{2n} (\varepsilon_1 - \varepsilon_m) (\varepsilon_d + \varepsilon_m) - (\varepsilon_m + \varepsilon_1) (\varepsilon_d - \varepsilon_m)}{\det_n}, \\ B_n &= \frac{2d_{2n} (\varepsilon_d + \varepsilon_m)}{\det_n}, \quad C_n = \frac{2(\varepsilon_m - \varepsilon_d)}{\det_n}, \quad D_n = \frac{4d_{2n} \varepsilon_m}{\det_n}, \end{aligned} \quad (12)$$

that completely determine the electric field inside, in, and out of the plasmonic ring. The determinant \det_n of Eq. (11) that is the denominator in Eq. (12) is equal to

$$\det_n = d_{2n} (\varepsilon_m + \varepsilon_1) (\varepsilon_m + \varepsilon_2) + (\varepsilon_1 - \varepsilon_m) (\varepsilon_m - \varepsilon_d). \quad (13)$$

Zeroing of the determinant $\det_n = 0$ gives the condition for the n th resonance exciting in the plasmonic ring. For the given permittivities of the metal ring ε_m , outer space ε_d , and the internal space ε_1 the ring resonates when its thickness takes the following values:

$$\begin{aligned} d_{0\text{res},n} &= r_0 \operatorname{Re} \left[\left(\frac{(\varepsilon_1 - \varepsilon_m)(\varepsilon_d - \varepsilon_m)}{(\varepsilon_m + \varepsilon_1)(\varepsilon_d + \varepsilon_m)} \right)^{\frac{1}{2n}} - 1 \right] \\ &\simeq r_0 \left[\left(\frac{(\varepsilon_1 - \varepsilon_{m1})(\varepsilon_d - \varepsilon_{m1})}{(\varepsilon_{m1} + \varepsilon_1)(\varepsilon_d + \varepsilon_{m1})} \right)^{1/2n} - 1 \right], \end{aligned} \quad (14)$$

where we restore natural dimensions and insert the radius r_0 of the ring, $n = 1, 2, 3, \dots$ is the resonance number, i.e., $2n$ is the number of nodes in the ring field $E^{(m)}$ (see Fig. 2). In the transition to the second estimation in Eq. (14), it is taken into account that the real part $\varepsilon_{m1} = \operatorname{Re}[\varepsilon_m]$ of the metal permittivity is much larger in absolute value than the imaginary part $\varepsilon_{m2} = \operatorname{Im}[\varepsilon_m] \ll |\varepsilon_{m1}|$ for the “good” optical metals like silver or gold. We obtain an expected result: the ring resonates if and only if the real part of the metal permittivity is negative. For the red and infrared parts of the optical spectrum, the real part ε_{m1} of the metal permittivity is negative and large in absolute value. Then, the dispersion equation, Eq. (14), simplifies to

$$d_{0\text{res},n} \simeq r_0 \frac{\varepsilon_d + \varepsilon_1}{n|\varepsilon_{m1}|}, \quad (15)$$

where r_0 is the radius of the ring. We obtain that the resonance thickness of the metal layer is inversely proportional to the absolute value of the metal permittivity.

The dimensionless intensity $\langle I^{(i)} \rangle$ of the resonance electric field averaged over the internal surface of the ring with thickness $d_{0\text{res},n}$ estimates as $\langle I^{(i)}(d = d_{0\text{res},n}) \rangle = I_{0\text{max},n} \simeq I_n$

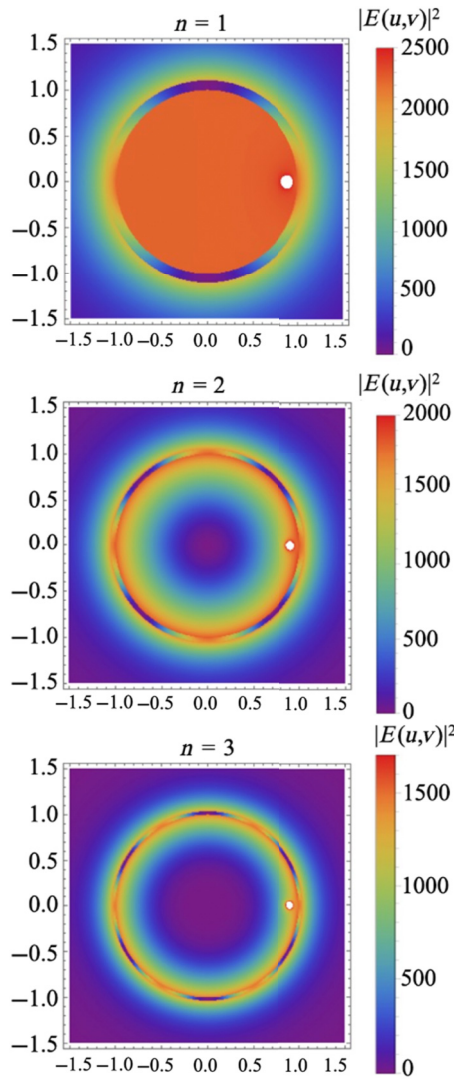


FIG. 2. Electric field in the silver ring for the plasmon resonances $n = 1, 2, 3$ at an excitation wavelength of $\lambda = 785$ nm. Silver permittivity is $\epsilon_m \approx -30 + 0.4i$, internal permittivity $\epsilon_1 = 1$, outer permittivity $\epsilon_d = 2$, ring thickness $d_{\text{res},n} = 0.11, 0.052, 0.034$, all dimensions are normalized to the ring radius r_0 . The white spot corresponds to the monopole, which is placed at $u = x_0 = 0.9, v = 0$.

from Eq. (8):

$$I_{0 \max,n} \simeq 2 \left[\frac{\epsilon_1 \epsilon_{m1} (\epsilon_d^2 - \epsilon_{m1}^2)}{\epsilon_{m2} (\epsilon_d + \epsilon_1) (\epsilon_{m1}^2 - \epsilon_1 \epsilon_d)} \right]^2 \left(\frac{x_0}{r_0} \right)^{2n}, \quad (16)$$

where n is the resonance number, $\epsilon_{m1} = \text{Re}\epsilon_m$, and $\epsilon_{m2} = \text{Im}\epsilon_m$. It follows from Eq. (16) the resonances have almost the same amplitude when the source is close to the ring, i.e., $x_0 \leq r_0$. Excitation of various resonances in the silver ring is illustrated in Fig. 2 for the wavelength $\lambda = 785$ nm. The silver permittivity for this wavelength is $\epsilon_m \simeq -30 + 0.4i$ [65], and the permittivity of the outer space is chosen to be $\epsilon_d = 2$, which corresponds to the

permittivity of the photoresist in our experiments. The first three resonances are displayed in Fig. 2. The electric field in a metal ring has two, four, and six nodes for the first, second, and third resonances, respectively. Note the first dipole resonance electric field, shown in Fig. 2(a), fills all the internal space of the ring. This result corresponds to the electric field distribution in the metal cylinder excited by a uniform external electric field [66]. A plasmon excited in a metal tube can be experimentally investigated. Suppose that the nanochannels with radius r_0 are formed in a dielectric material. Nanochannels can be produced, for instance, in the silicon by electrochemical etching (see Ref. [67] and references therein). The surface of the nanochannels is covered by a silver layer with the thickness $d_{\text{res},1} \simeq r_0(\epsilon_d + 1)/(|\epsilon_m|)$ given by Eq. (15). Suppose further that the Raman-active analyte is injected in these channels. Then, the Raman signal from the molecules in the nanochannels is much enhanced since the scattering is incoherent and the Raman intensities are summed up. The Raman enhancement factor (SERS) estimates as $G \sim I_{\max,n}^2$ (see, e.g., Ref. [68]), where $I_{\max,n} \gg 1$ is given by Eq. (16) and the parameter $x_0 \sim r_0$. For the typical Raman spectroscopy wavelength of $\lambda = 785$ nm, the silver permittivity is about $\epsilon_m \simeq -30 + 0.4i$ and the enhancement factor estimates as $G \sim (\epsilon_{m1}/\epsilon_{m2})^4 \sim 10^7$. This holds for any argument of the complex amplitude E_0 . For instance, in the case $E_0 = -2iQ$, $Q > 0$ the monopole potential (1) is the potential of the usual electric charge, for which density is equal to $Q\delta(u - x_0)\delta(v)$. Any other field sources such as a dipole or quadrupole can be combined from electric monopoles.

B. Giant electric field in metal grating

We consider a modulated metal film. The metal grating is placed at the plane $X = 0$. The electromagnetic wave propagates along X axis being “y” polarized, i.e., $E \sim \{0, E_0, 0\} \exp(ikX)$, where $k = \omega/c$ is the wave vector. The wave impinges on the front surface of the grating, where the plasmon is excited due to the modulation [see Fig. 3(a)]. In this section devoted to the analytical consideration, we assume that the film modulation h , as well as its period L , are much smaller than the wavelength $\lambda = 2\pi/k$. In this case, we can approximate $E \sim \{0, E_0, 0\} \exp(ikX) \simeq \{0, E_0, 0\}$ that is the plasmon grating is excited by uniform field E_0 , which is y directed and oscillates with frequency ω . It is convenient to introduce the complex variable $Z = X + iY$. We use the quasistatic approach, therefore, the incident field is described by the complex potential $\varphi(Z) = iZE_0$, where we assume that the field E_0 takes real values. Then, $E_x = -\text{Re}[d\varphi(Z)/dZ] = 0$, $E_y = \text{Im}[d\varphi(Z)/dZ] = E_0$ (see Fig. 3). It is convenient to shift from the real coordinates X and Y to the dimensionless coordinates x and y that are defined by using the period of the film modulation L , namely, $x = 2\pi X/L$ and

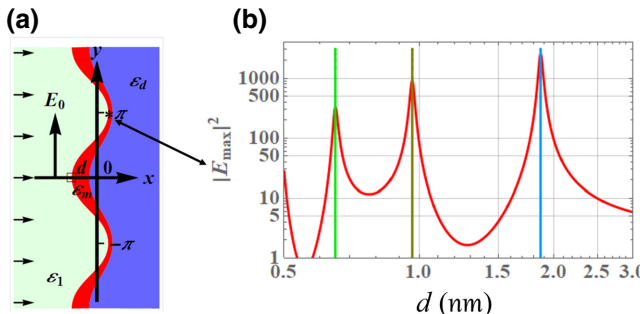


FIG. 3. (a) The design of plasmonic grating based on a metal film with a permittivity ϵ_m deposited on the modulated dielectric substrate (shown in blue) with a permittivity ϵ_d , metal film has thickness d , “y”-polarized light is incident from left; star “*” denotes the point with coordinates $x = x_{\max}^{(f)}$ and $y = \pi$, where surface electric field has maximum; small open square “□” denotes the point with coordinates $x = x_{\min}^{(f)}$ and $y = 0$, where surface electric field has minimum, the film modulation $h = (x_{\max}^{(f)} - x_{\min}^{(f)})L/2\pi$. (b) Intensity of local electric field at surface of silver film, which is modulated with period L ; the field is shown in the point $X_{\max} = x_{\max}^{(f)}(L/2\pi)$ and $Y_{\max} = \pi(L/2\pi)$ [star “*” in (a)] as function of the film thickness d , where the period is equal to $L = 50$ nm, amplitude of the modulation is equal to $h = 11$ nm, silver permittivity is equal to $\epsilon_m \approx -30 + 0.4i$ at 785 nm, permittivity of dielectric substrate is equal to $\epsilon_d = 2$, permittivity of front medium $\epsilon_1 = 1$. Vertical color lines correspond to plasmon resonances given by Eq. (25).

$y = 2\pi Y/L$. That is the periodically modulated metal film has a “natural” period of 2π being considered in x and y frame as shown in Fig. 3(a). Recall we use the quasistatic approximation since the amplitude of metal modulation is assumed to be much smaller than the wavelength of the incident light. The potential φ of the local electric field does not change after rescaling of the coordinates, since there is no characteristic length in the Laplace equation:

$$\varphi(z) = izE_0, \quad (17)$$

where $z = x + iy$. The shape of the modulated metal film is chosen in such a way that the front surface $\{x_f, y_f\}$ of the modulated metal film [left red surface in Fig. 3(a)] is given by the parametric equation, which is convenient to write in a complex form

$$z^{(f)}(\phi) = x^{(f)}(\phi) + iy^{(f)}(\phi) = \ln[\exp(i\phi) - x_0], \quad (18)$$

where the parameter x_0 takes values in the interval $0 < x_0 < 1$, the variable ϕ changes in the limits $-\infty < \phi < \infty$; the logarithm is the full analytical function defined in all Riemann surfaces so that y also varies within the limits of $-\infty < y < \infty$. The back surface $x_b(\phi) > x_f(\phi)$ of the metal film [right red surface in Fig. 3(a)] is given by the

parametric equation:

$$\begin{aligned} z^{(b)}(\phi) &= x^{(b)}(\phi) + iy^{(b)}(\phi) \\ &= \ln[(1 + d_0)\exp(i\phi) - x_0], \end{aligned} \quad (19)$$

where the parameter ϕ still changes in the limits $-\infty < \phi < \infty$. The shape of the metal film is fully defined by its period L , the amplitude of the modulation $h = (x_{\max}^{(f)} - x_{\min}^{(f)})L/2\pi$, and the largest film thickness $d = (x_{\max}^{(b)} - x_{\min}^{(b)})L/2\pi$. The parameters d_0 and x_0 in Eqs. (18) and (19) are expressed in terms of the film modulation h and the film thickness d , namely,

$$x_0 = \tanh\left(\frac{h_1}{2}\right), \quad d_0 = 2 \frac{\exp(d_1) - 1}{\exp(h_1) + 1}, \quad (20)$$

where $h_1 = h(2\pi/L)$ and $d_1 = d(2\pi/L)$. Therefore, the period L , the modulation h , and thickness d completely determine the shape of the modulated metal film indeed. Note that the film defined by Eqs. (18) and (19) mimics a metal film obtained, for example, by the metal evaporation on the modulated dielectric substrate. During the deposition process, the metal concentrates on tops of the film [see Fig. 3(a)]. The thickness of metal on the tops of the grating (square “□” in Fig. 3) is larger than the thickness in the depressions (star “*” in Fig. 3). The difference in metal thicknesses increases with increasing the film modulation since the peaks shade the valleys in the process of the metal evaporation and deposition. The film can be profiled “artificially” using, e.g., the mask deposition.

To find the optical electric field in and around a modulated metal film, illuminated by the incident light, we use coordinates u and v that are convenient to introduce in the complex form:

$$w = u + iv = \exp(z) + x_0, \quad (21)$$

where $z = x + iy$. In the transition from x, y frame to u, v frame, the whole metal film transforms to the ring $1 \leq |w| \leq 1 + d_0$. The front and back surfaces of the grating are transformed to the internal $|w| = 1$ and outer $|w| = 1 + d_0$ surface of the ring. All the space in front of the grating [left from the grating in Fig. 3(a)] transforms in the space inside the ring $|w| < 1$ in Fig. 1(a), the space behind the grating [right from the grating in Fig. 3(a)] transforms into the outer space of the ring $|w| > 1 + d_0$. That is the metal film in Fig. 3(a) is rolled into a metal tube in Fig. 1. The approach is similar to the map used in Refs. [30,49]. The electric potential given by Eq. (17) transforms in $\{u, v\}$ frame to the potential φ_{sing} in Eq. (1). Therefore, the complex electric potential $\varphi(z)$ for a modulated metal film equals $\varphi[w(z)]$, where $\varphi(w)$ is the potential, which is found in the previous subsection for the metal ring. The complex electric field inside

and around the modulated metal film is obtained from the following equation: $\tilde{E}(z) = E_x - iE_y = -d\varphi[w(z)]/dz = [-d\varphi(w)/dw][dw/dz] = [dw/dz]\tilde{E}(w)$, where the complex field $\tilde{E}(w)$ is given by Eqs. (3)–(7) and (12). The equation for the electric field E_x, E_y can be rewritten in the matrix form as follows:

$$\begin{bmatrix} E_x(x,y) \\ E_y(x,y) \end{bmatrix} = \begin{bmatrix} r - \frac{ux_0}{r} & \frac{vx_0}{r} \\ -\frac{vx_0}{r} & r - \frac{ux_0}{r} \end{bmatrix} \begin{bmatrix} E_r(u,v) \\ E_\phi(u,v) \end{bmatrix}, \quad (22)$$

where $\{E_x, E_y\}$ is the field in the metal film [see Fig. 3(a)], $\{E_r, E_\phi\}$ are radial and angular components of the field are given by Eq. (7), which is found for the plasmon resonance in the metal nanoring (see Fig. 2), $r \equiv |w| = \sqrt{u^2 + v^2}$ is the radius in $\{u, v\}$ frame. The values of $u = \exp(x) \cos(y) + x_0$ and $v = \exp(x) \sin(y)$ are obtained from Eq. (21). Below, we suppose that $E_0 = 1$ and measure all fields in terms of the applied field. The local electric field at the modulated metal surface is shown in Fig. 3(b) in the point with coordinates

$$X_{\max} = (L/2\pi)x_{\max}^{(f)} = (L/2\pi) \ln(1 + x_0) \quad (23)$$

and

$$Y_{\max} = L/2 + mL \quad (m = 0, \pm 1, \pm 2, \dots) \quad (24)$$

as a function of the film thickness d (see * in Fig. 3a). The wavelength of the incident light is $\lambda = 785$ nm. The film is deposited on the dielectric with permittivity ε_d , and the permittivity of the front medium $\varepsilon_1 = 1$. The surface electric field is much enhanced for the film thickness corresponding to the excitation of plasmon resonances. The resonance thickness $d_{\text{res},n}$ is obtained from Eqs. (14) and (20):

$$d_{\text{res}} = \frac{L}{2\pi} \ln \left[\frac{\left(\frac{(\varepsilon_1 - \varepsilon_{m1})(\varepsilon_d - \varepsilon_{m1})}{(\varepsilon_1 + \varepsilon_{m1})(\varepsilon_d + \varepsilon_{m1})} \right)^{1/2n} - \tanh \frac{h_1}{2}}{1 - \tanh \frac{h_1}{2}} \right], \quad (25)$$

where L is the period and $h_1 = h(2\pi/L)$ is the dimensionless film modulation. The resonances are indicated by vertical lines in Figs. 3(b) and 6(a). The distributions of the local electric field for the three resonances are displayed in Fig. 4. The local electric field is much enhanced and exceeds the incident field E_0 by 2–3 orders on the magnitude. The enhanced field spreads over the grating achieving its maxima in the depressions of the front surface. The amplitude of the maximum field in the point with coordinates X_{\max}, Y_{\max} at the front surface of the metal film [star “*” in Fig. 3(a)] is given by the following equation obtained from Eq. (7) by substitution there $r = 1$ and $f = \pi$ and multiplying the result by matrix (22)

$$E_x(X_{\max}, Y_{\max}) = E_0(1 - x_0) \left[\frac{1}{1 + x_0} + \sum_{n=1}^{\infty} (-x_0)^n \frac{(\varepsilon_1 + \varepsilon_m)(\varepsilon_m - \varepsilon_d) + (d_0 + 1)^{2n}(\varepsilon_1 - \varepsilon_m)(\varepsilon_d + \varepsilon_m)}{(\varepsilon_1 - \varepsilon_m)(\varepsilon_m - \varepsilon_d) + (d_0 + 1)^{2n}(\varepsilon_1 + \varepsilon_m)(\varepsilon_d + \varepsilon_m)} \right],$$

$$E_y(X_{\max}, Y_{\max}) = 0, \quad (26)$$

where the parameters x_0 and d_0 are given by Eq. (20). The useful characteristic is the amplitude of the resonance field averaged over the surface of the metal film, which has resonance thickness $d_{\text{res},n}$ given by Eq. (25). The amplitude is still given by Eq. (16), where the ratio x_0/r_0 is replaced by $\tanh h_1/2$. For the practically useful case $|\varepsilon_m| \gg \varepsilon_d$, the averaged intensity at the n th resonance is estimated as follows:

$$I_{\max,n} \sim \left[\frac{\varepsilon_1 \varepsilon_{m1}}{\varepsilon_{m2} (\varepsilon_d + \varepsilon_1)} \tanh^n \frac{\pi h}{L} \right]^2, \quad (27)$$

where we skip numerical coefficient on the order one.

Resonance optical properties of a metasurface are defined by moments of the fluctuating local electric field $E(\omega)$. For instance, the electromagnetic enhancement of

the Raman signal, i.e., SERS effect is given by the following [68]:

$$G(\omega, \Delta\omega) = \frac{1}{|E_0|^4} \langle |E(\omega)|^2 |E(\omega - \Delta\omega)|^2 \rangle$$

$$\simeq \frac{1}{|E_0|^4} \langle |E(\omega)|^4 \rangle \simeq \frac{1}{|E_0|^4} \langle |E(\omega - \Delta\omega)|^4 \rangle, \quad (28)$$

where ω is the laser frequency, $\omega - \Delta\omega$ is the frequency of the Raman spectral line, $\Delta\omega \ll \omega$ is known as Stokes shift, brackets $\langle \dots \rangle$ denote the spatial average, E_0 is the amplitude of the incident light. The average in Eq. (28) goes over the volume filled with the Raman active molecules. When the molecules of an analyte are distributed over the surface the average reduces to the

integration over the surface of the metal grating. Suppose that the metal grating, shown in Fig. 3, is illuminate with frequency ω , the metal thickness has the resonance value $d = d_{\text{res}}$, given by Eq. (25). The local electric field

$E(\omega)$ is given by Eqs. (7), (11), and (22). Integration over the film surface results in the following Raman enhancement G in the modulated metal film that have resonance thickness

$$G(\omega, \Delta\omega) \simeq \frac{16\varepsilon_1^4 \varepsilon_{m1}^4 (\varepsilon_d - \varepsilon_{m1})^2 (\varepsilon_d^2 - \varepsilon_{m1}^2)^2 [3 \cosh(\frac{4\pi h}{L}) + 1] \operatorname{sech}^4(\frac{\pi h}{L}) \tanh^{4n}(\frac{\pi h}{L})}{(\varepsilon_d + \varepsilon_1)^2 (\varepsilon_1 + \varepsilon_{m1})^2 (\varepsilon_{m1}^2 - \varepsilon_1 \varepsilon_d)^2} \frac{1}{\varepsilon'_{m1}^2 \Delta\omega^2 + \varepsilon_{m2}^2}, \quad (29)$$

where $\varepsilon_{m1} = \operatorname{Re}\varepsilon_m(\omega)$, $\varepsilon_{m2} = \operatorname{Im}\varepsilon_m(\omega) \ll |\varepsilon_{m1}|$, and $\varepsilon'_{m1} = \partial\varepsilon_{m1}/\partial\omega$, are real, imaginary, and derivative of the metal permittivity, L and h are period and modulation of the metal grating, $n = 1, 2, \dots$ is the resonance order. We assume that permittivities ε_d and ε_1 are real and can be considered as constant for the Stokes shift $|\Delta\omega| \ll \omega$. The enhancement G is shown in Fig. 5 as function of the Stokes shift. For the laser wavelength $\lambda = 785$ nm, the enhancement factor G exceeds 10^5 for Stokes shift $|\Delta\omega| < 10^3$ cm $^{-1}$. Therefore, the discussed film can be used as SERS sensor to detect various analytes as 4-mercaptophenyl boronic acid (discussed in Sec. IV B), for instance. The metal grating can be tuned to the intermediate resonance frequency ω_r , which is smaller than the laser frequency. Then, the silver grating presented in Fig. 5 could enhance the Raman spectral lines with Stokes shift $\Delta\omega$ up to 2000 cm $^{-1}$ and more.

Any real metal grating has dispersion in local parameters including the film thickness and modulation. Local geometric parameters fluctuate for any method of the manufacturing. The dispersion of the local parameters

results in inhomogeneous broadening of the plasmon resonances. Then the spectral range, where the metal grating works as SERS sensor, also increases. Yet, the enhancement of the working band comes at the expense of the SERS value.

The analytical results are compared with the results of computer simulations. Computer simulations are performed for the electromagnetic field distribution in a weakly profiled silver film deposited on a photoresist. The dimensions of the computer model are the same as those described in Figs. 3(b) and 4 ($\varepsilon_1 = 1$, $\varepsilon_d = 2$, i.e., the refractive index of the photoresist is $n = 1.41$). The simulations are done in COMSOL environment. The Maxwell equations are solved by the finite-element method. We demonstrate the enhancement of the electric field $|E/E_0|^2$ in the modulated thin metal film with period $L = 50$ nm and amplitude of the modulation $h = 11$ nm (see Fig. 6). It can be seen that positions of the analytical and numerical resonances are in good agreement. The distribution of the electric field for two resonances shown in Fig. 6(a)

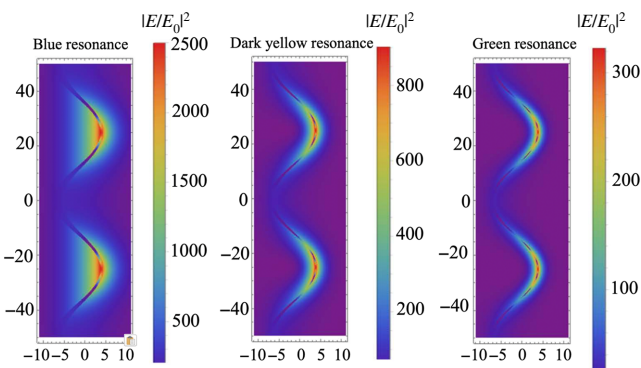


FIG. 4. Local electric field in a modulated silver film for the blue, dark yellow, and green resonances displayed in Fig. 3(b), where the period is $L = 50$ nm, modulation amplitude is $h = 11$ nm, silver permittivity at $\lambda = 785$ nm is $\varepsilon_m = -30 + 0.4i$, permittivity of dielectric substrate is $\varepsilon_d = 2$, and permittivity of front space $\varepsilon_1 = 1$.

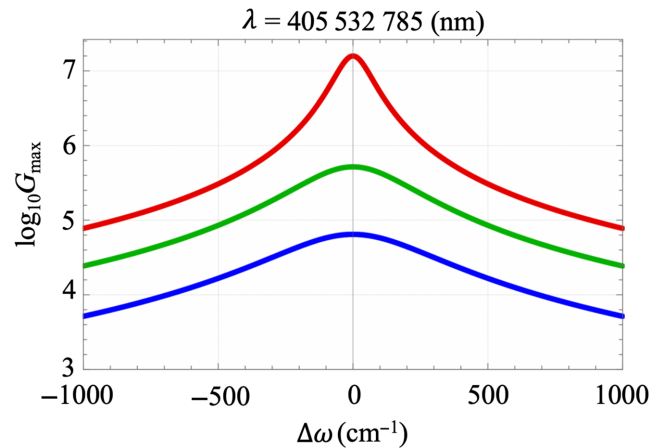


FIG. 5. SERS factor G for modulated silver film as function of the Stokes shift $\Delta\omega$, laser frequency $\omega = 24\,691, 18\,797$, and $12\,739$ cm $^{-1}$ ($\lambda = 405, 532$, and 785 nm, respectively): blue, green, and red lines with the following parameters: film period $L = 50$ nm, modulation $h = 11$ nm, and silver permittivity is from [65], $\varepsilon_d = 2$, $\varepsilon_1 = 1$.

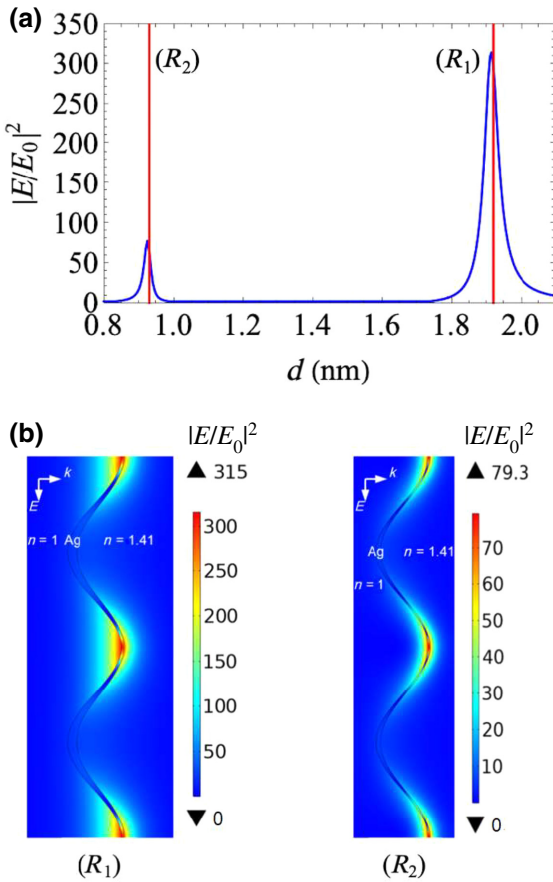


FIG. 6. (a) Electric field intensity for different thicknesses d of the silver film (illumination under normal incidence, with the following parameters: $L = 50$ nm and $h = 11$ nm; $\lambda = 785$ nm). The red vertical lines indicate resonance thicknesses obtained from analytical theory. (b) Distributions of the electric field intensity corresponding to two resonances (R_1) and (R_2).

is displayed in Fig. 6(b). Our analytical theory is in agreement with the computer simulations (see the resonances in Figs. 4 and 6). We also simulate the resonant enhancement of the electric field for a modulated metal film whose parameters correspond to the experiment discussed below (see Fig. 7). Figures 7(a) and 7(b) show the computer simulations and result of the analytical theory [Eq. (26)]. Resonances are due to the excitation of dipolar and multipolar plasmons in the modulated metal film. The electric field distribution in dipolar and multipolar plasmons is in qualitative agreement with analytical theory [see the resonances: (I), (II), and (III) displayed in Figs. 7(a) and 7(b)]. The field distribution in the resonance (IV) in Figs. 7(b) and 7(c) differs from all other resonances. The electric field expands from the metal surface at a distance comparable with the wavelength and period of the modulation. We speculate that in this case, the plasmon resonance hybridizes with plasmon propagating over the

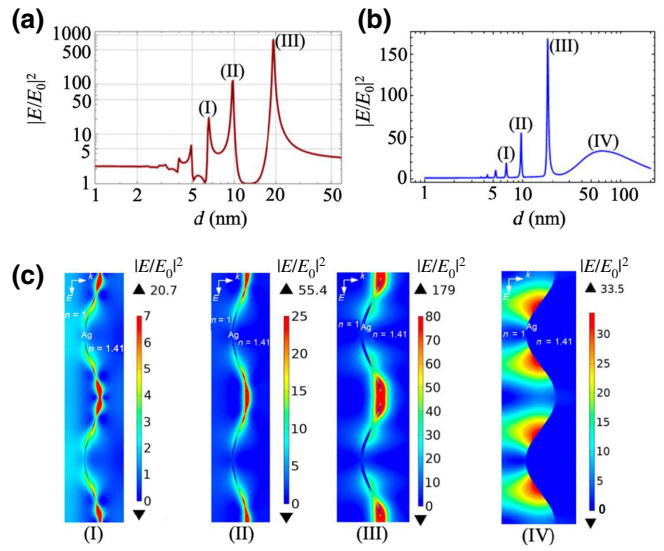


FIG. 7. Intensity of electric field for different thicknesses of silver film d with the following parameters: period $L = 750$ nm and amplitude of the modulation $h = 100$ nm (illumination at $\lambda = 785$ nm, under normal incidence), calculated by using (a) the result of Eq. (26) and (b) computer simulations. (c) Computer simulation of distribution of local electric field corresponding to resonances: (I) $d = 6.75$ nm, (II) $d = 9.6$ nm, (III) $d = 17.9$ nm, and (IV) $d = 70$ nm.

modulated metal surface (see Ref. [43]). The hybridization could be the subject for further consideration.

In summary, we present the analytical theory of plasmons excited in a modulated metal film deposited on a dielectric substrate. Computer simulations and results of the analytical theory are in good agreement. The resonance conditions are found as a function of the metal permittivity, modulation, and thickness of the film. When the grating is excited by the incident light, the surface electric field is much enhanced. The quasistatic theory qualitatively described the field enhancement even in the case $kL \simeq 1$, since the field is concentrated in the nanograting whose thickness and modulation are much smaller than λ . The size of a plasmon maxima l_p is on the order of the film modulation $l_p \approx h$ (see Figs. 4, 6, and 7). The radiation loss, which is proportional to $l_p dk^2$ remains to be less than one. For example, for silver film with parameters $h = 100$ nm, $d = 20$ nm, and $\lambda = 785$ nm (see Fig. 7), $l_p dk^2 \approx 0.1 < 1$. The positions of the plasmon resonances from computer simulations almost coincide with the results of Eq. (25). The resonance enhancement of the electric field obtained in computer simulations is fairly large. Yet, the computer results are a few times smaller than the results of the quasistatic equation, Eq. (26). The discrepancy is due to the radiation loss that can be taken into account by using a perturbation theory. Yet, we do not expect a qualitative difference between the quasistatic approximation

and exact result while plasmons are localized like in resonances (I)–(III) (Fig. 7). The developed analytical theory can be used for the design of alternative SERS substrates and other optical sensors. The theory can be extended to multilayered metal-dielectric films.

We also perform a computer simulation of the rectangular dielectric grating covered by the thin metal film. It is interesting to note that plasmon resonances in the rectangular grating are rather similar to that discussed above [see Figs. 6, 7, and 8(a)]. Indeed, for the fixed wavelength, the local electric field achieves maximum at the resonance thickness of the metal film that covers the rectangular grating [see Fig. 8(a)]. The resonance field concentrates in the bottom of rectangular wells, and the number of nodes increases with decreasing the thickness of the metal film as clearly seen in Fig. 8(b). The gratings' parameters are taken similar to the calculations for Fig. 7 (period, $L = 750$ nm; rectangle height, $h = 100$ nm; rectangular width, $D = 375$ nm). The thickness of the silver on the side walls is assumed to be 2 times smaller than on the

top and it is about 4 times less at the bottom of a well than on the top. The rectangular grating might be better suited for accepting the analyte solution that has an opportunity to concentrate at the bottom of the wells. The grating with a profile close to the rectangular can be obtained by photolithography using a nonlinear photoresist (e.g., Microposit S1800 G2).

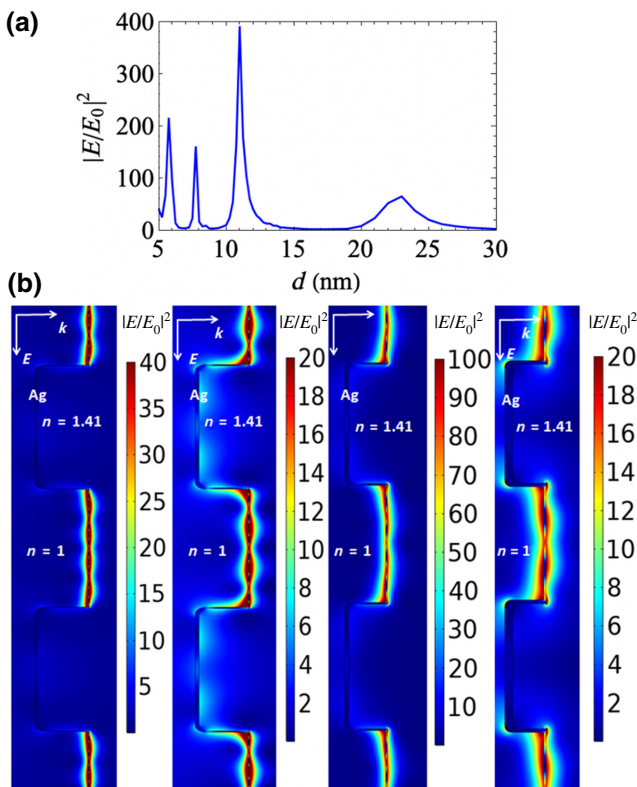


FIG. 8. For different thicknesses of the silver film d in rectangular metal grating, intensity of electric field is displayed in (a), and distribution of electric field in (b) (from left to right: $d = 5.75$ nm, $d = 7.75$ nm, $d = 11$ nm, $d = 14.6$ nm, and $d = 23$ nm) with the following parameters for the rectangular grating: period $L = 750$ nm, rectangle height $h = 100$ nm, rectangle width $D = 375$ nm [illumination at $\lambda = 785$ nm for (a) and left-side lighting at $\lambda = 785$ nm for (b), both under normal incidence].

C. Plasmon resonances in three-dimensional metal grating

We briefly consider now plasmon resonances in the double periodic metal grating obtained by deposition of the thin metal film on the double periodic dielectric substrate. At the moment, we cannot analytically calculate the local electric field in this actually three-dimensional structure even using quasistatic approximation. Instead, the amplitude of the local field $|E/E_0|^2$ is found from the direct numerical solution of the Maxwell equations in the COMSOL environment. We simulate the enhancement of the electric field in the modulated thin metal film with period $L = 760$ nm and amplitude of the modulation $h = 30$ nm [see Fig. 9(a)]. Figure 9(b) shows the computer simulation of the distribution of the electric field intensity in resonant thicknesses of the silver film. Resonances are due to the excitation of “dipolar” and “multipolar” plasmons in the modulated metal film with metal thicknesses of $d = 25$ nm, $d = 14.6$ nm, and $d = 11.3$ nm on the top of the grating, displayed in Fig. 9(b). These resonances are similar to resonances presented in Fig. 6. We speculate that the additional “magneticlike resonances” are excited in a doubly periodic structure with metal thicknesses of $d = 17.4$ nm, $d = 13.3$ nm, and $d = 10.4$ nm in Fig. 9(b). Interestingly, the developed analytical theory describing the excitation of plasmon resonances in the simplest two-dimensional grating gives an insight into plasmon resonances in the 3D full-sized structure of the open resonators.

III. EXPERIMENTAL INVESTIGATION OF OPEN RESONATOR-METASURFACES

A. Fabrication process

The metasurfaces are fabricated by the following steps. As a first step $1.5 - 1.9 \mu\text{m}$ recording layer of positive photoresist (Microposit S1800) is deposited by spin coating on the silicon wafer. Then, 15 areas of two-dimensional modulated films ($1.5 \times 1.5 \text{ cm}^2$) are formed by the holographic lithography technique. The schematic diagram of recording setup employs a phase-modulator HED-6001 Monochrome LCoS microdisplay, and an ultraviolet laser ($\lambda = 405$ nm)

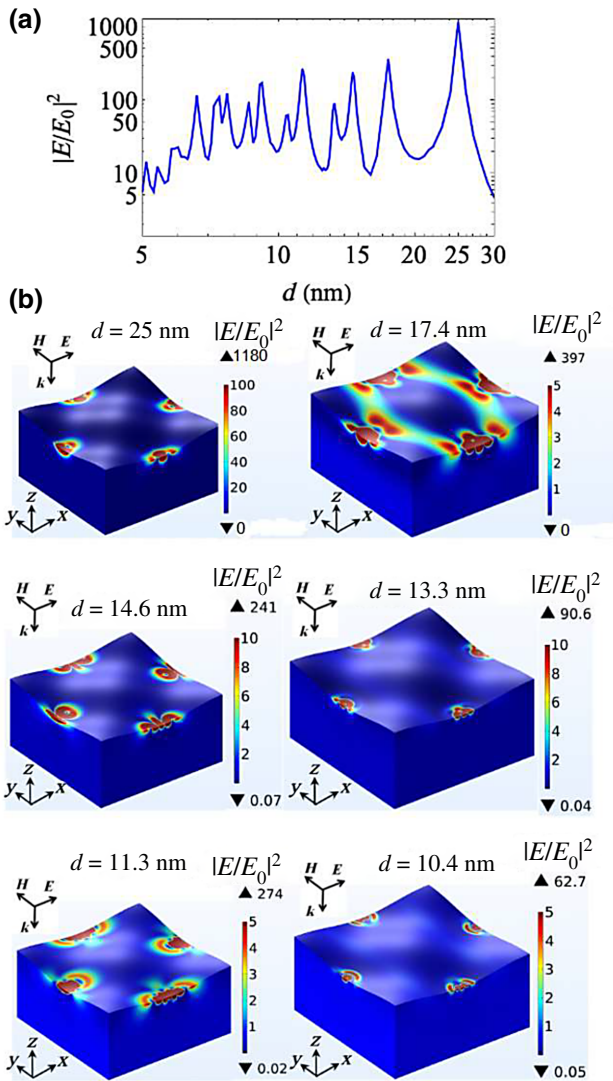


FIG. 9. For different thicknesses of the silver film d in 3D metal grating, intensity of electric field is displayed in (a), and distribution of electric field in (b) with the following parameters for the 3D grating: period $L = 760$ nm, modulation amplitude $h = 30$ nm (illumination at $\lambda = 785$ nm, under normal incidence).

[see Fig. 10(a)]. The exposure dose is varied from 4.1 to $8.5 \mu\text{J}/\text{cm}^2$. The angle between interfering light waves is around 49° . Next, the resist is developed in Microposit 303A developer. Afterwards, two successive depositions of a 80-nm SiO_2 layer and a 30-nm silver layer are realized by electron-beam evaporation. The metasurfaces with periods from 720 to 770 nm and modulation amplitude from 8 to 30 nm are fabricated [see Fig. 10(b)]. The sketch of the metasurface morphology is shown in Fig. 10(c). The morphology of the fabricated metasurfaces is measured with a scanning electron microscopy (SEM, JEOL), and SEM images of these metasurfaces are shown in Figs. 10(d) and 10(e). Finally, modulation amplitude measurements

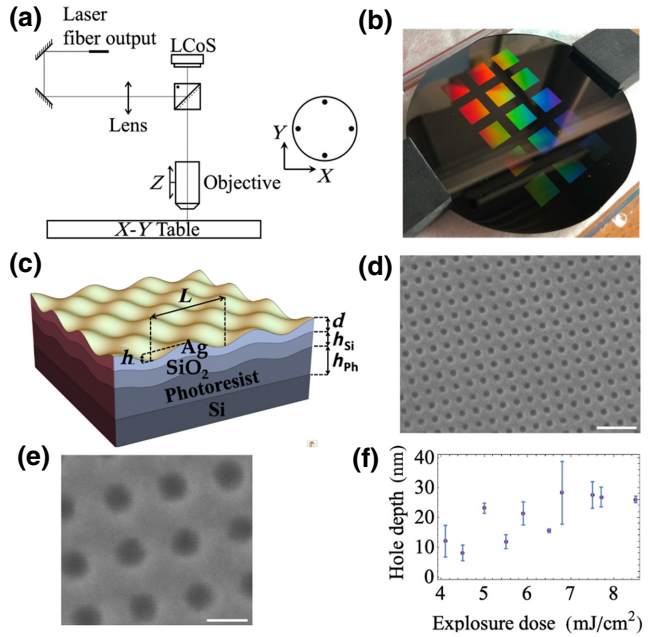


FIG. 10. (a) Principle scheme of the recording setup. (b) Photo of 4-in. wafer where metasurfaces are fabricated. (c) Principle scheme of the metasurface design with the following parameters: period is $L = 720 - 770$ nm, modulation amplitude is $h = 8 - 30$ nm, silver layer thickness is $d = 30$ nm, thickness of SiO_2 is $h_{\text{Si}} = 80$ nm, photoresist thickness is $h_{\text{ph}} = 1.5 - 1.9 \mu\text{m}$. SEM images of the metasurfaces (period $L \approx 760$ nm, and film modulation $h \approx 30$ nm) with a scale bar of $2 \mu\text{m}$ for (d) and 500 nm for (e). (f) Hole depth versus exposure dose (depth measured by AFM).

are made with an atomic force microscopy (AFM; Solver Pro NT-MDT) for different exposure doses [see Fig. 10(f)].

B. Deposition of 4-mercaptophenylboronic acid for SERS

In order to study the sensitivity of the metasurfaces, we employ molecules of 4-mercaptophenylboronic acid (4-mPBA), which are small molecules (thickness of a 4-mPBA monolayer is around 0.8 nm [69]). We choose boronic acid, which is a specific substance because the boron group covalently binds diols and forms a boron ester. Therefore, boronic acid is considered as a specific agent for sugars and their fragments. There is a strong covalent fixation of this acid on the surface of silver due to the thiol group ($-SH$). The analyzed molecules are covalently bound to the silver, thereby increasing the probability of the location of molecules in the region of generation of giant electromagnetic fields. In addition, we prepare solutions of 4-mPBA in ethanol with concentrations varying from 2.3×10^{-8} M to 2.3×10^{-3} M. Then, for SERS experiments, an aliquot of each 4-mPBA solution is applied onto the metasurface and then dried at room temperature. Finally, the 4-mPBA concentration employed for Raman measurements in solution (ethanol) is 0.5 M.

C. Reflectance and Raman measurements

For characterizing the optical properties of metasurfaces, the reflectance spectra are recorded by using a spectroscopic ellipsometer SE 850 DUV (Sentech, Germany). For the SERS measurements, a Raman spectrometer Inno-Ram (BWTek, USA) with an excitation wavelength of 785 nm and a spectral resolution of 4 cm^{-1} is employed. The acquisition time and the laser power are set at 1 s and 3.84 mW, respectively. The laser spot has a diameter of $1.2 \mu\text{m}$ (spot area approximately equal to $1.1 \mu\text{m}^2$) at the excitation wavelength. A microscope objective ($\times 50$, NA = 0.8) is used in order to focus the laser beam on the metasurface, and the Raman signal of the 4-mPBA molecules immobilized on the metasurface is detected by the same objective in a backscattering configuration. In addition, for Raman measurements in solution, the same setup is used. For the acquisition time and the laser power, we fix them at 2 s and 2.5 mW, respectively.

IV. RESULTS AND DISCUSSION

A. Optical properties of metasurfaces

To determine the macroscopic optical properties of metasurfaces, the angular reflectance spectrum is measured by ellipsometry in the range from 20° to 70° . The reflectance spectrum is measured for two polarizations: R_p for p polarization of the incident light and R_s for s polarization of the incident light. The measured reflectance spectra for R_p and R_s show deep gaps with a complex behavior versus period and angle (see Fig. 11).

Raman instruments are usually attached to microscopes, where the excitation and the inelastically scattered light are delivered. The light is collected from the sample through the same objective in backscattering geometry.

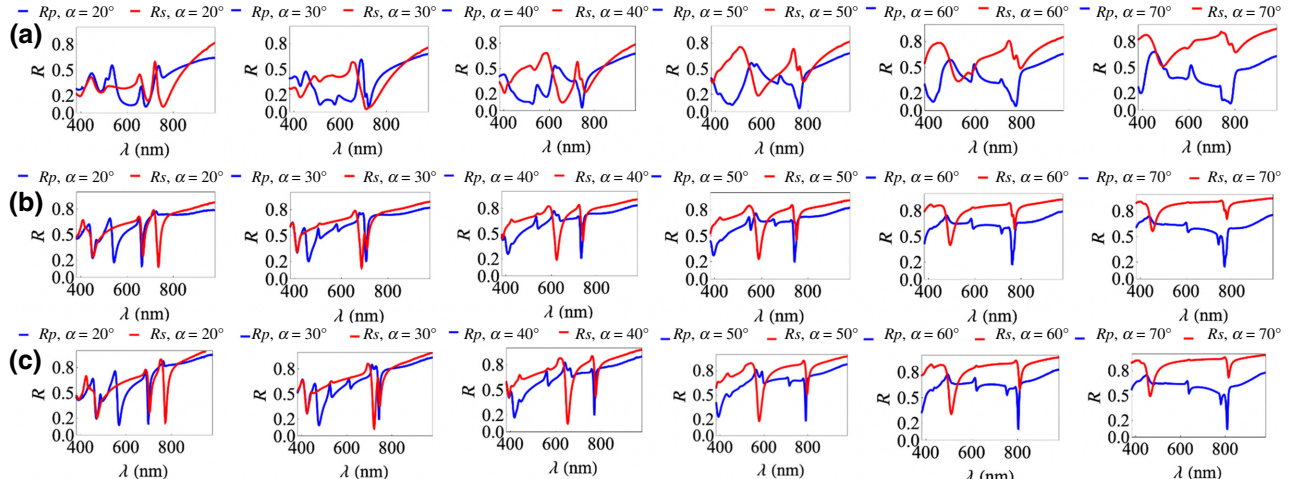


FIG. 11. Experimental angular reflectance spectra from the metasurface for different angles of the incident light and with the following structure parameters: (a) $L = 720 \text{ nm}$, depth $h \approx 30 \text{ nm}$; (b) $L = 720 \text{ nm}$, depth $h \approx 20 \text{ nm}$; (c) $L = 770 \text{ nm}$, depth $h \approx 18 \text{ nm}$.

The objective is characterized by a NA equal to 0.8 in our case. This means that the cone angle is equal to $2\alpha = \arcsin(\text{NA}) = 106^\circ$. So, we have to take into account all the rays of the incident light at angles α from 0° to 53° . The focal length f is related to the lens diameter by the ratio $(D/2f) = \tan \alpha$ (D , lens diameter). We find the average reflection in the approximation of the geometric optics by integrating the reflection over the basis of the cone of the incidence. The schematic drawing of the polarized light collected by the lens is displayed in Fig. 12(a). The average reflection is expressed as follows:

$$R_{\text{average}} = 2 \left(\frac{1}{\text{NA}^2} - 1 \right) \int_0^{\alpha_{\text{max}}} \frac{\sin \alpha}{\cos \alpha^3} R(\alpha) d\alpha, \quad (30)$$

where $\alpha_{\text{max}} = \arcsin(\text{NA})$. In addition, each ray has a transverse and longitudinal field component, so we average R_p and R_s . The resulting average reflection is displayed in Fig. 12(b). We observe minima on the spectral range from 400 to 800 nm and more specifically close to the excitation wavelength of 785 nm. We assume that these minima in the reflectance spectrum correspond to plasmon resonances. These plasmonic resonances (close to the excitation wavelength of 785 nm) will permit the enhancement of the Raman signal of 4-mPBA molecules.

B. SERS detection of 4-mercaptophenylboronic acid molecules

For all the SERS experiments, a modulated silver metasurface with a period $L = 760 \text{ nm}$, $h = 30 \text{ nm}$ is used. This metasurface has the maximum available modulation depth $h = 30 \text{ nm}$. With a higher modulation depth, the number of electromagnetic modes increases. Thus, this modulation allows obtaining deep minima in the reflectance spectrum close to the excitation wavelength of 785 nm [see

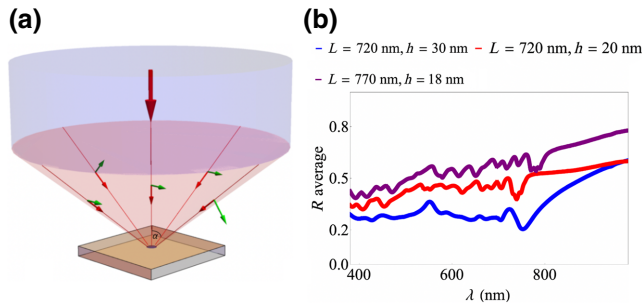


FIG. 12. (a) Schematic illustration of the polarized light impinged to the sample by the lens. The red and green arrows show the directions of the wave vector and the electric field, respectively. (b) Average experimental reflectance spectra from modulated silver film (metasurface), the reflectance is averaged over the light cone, which is focused by the Raman microscope on the sample.

Fig. 12(b)]. Then, to evaluate the sensitivity of these metasurfaces, 4-mPBA molecules are grafted onto them by using the functionalization protocol described in Sec. III B. Next, the SERS spectra have been recorded at the excitation wavelength of 785 nm.

Figure 13 shows the SERS spectra of 4-mPBA molecules on metasurfaces obtained for each concentration varying from 2.3×10^{-8} M to 2.3×10^{-3} M. From the SERS spectrum obtained for the concentration of 2.3 mM depicted in Fig. 13, seven characteristic Raman peaks of 4-mPBA molecules are well distinguished [63,70,71]. The Raman peaks at 420, 693, and 1072 cm^{-1} correspond to the C-C-C in-plane bending mode coupled with C-S stretching mode (called, respectively, β_{CCC} and ν_{CS}). Then, the peak at 480 cm^{-1} corresponds to the C-C-C out-of-plane bending mode coupled to O-B-O in-plane bending mode (called, respectively, γ_{CCC} and β_{OBO}). The Raman peaks at 1000 cm^{-1} and 1030 cm^{-1} correspond, respectively, to the C-C-C in-plane bending mode (called β_{CCC}) and the C-H in-plane bending mode (called β_{CH}). Finally, the Raman peak at 1580 cm^{-1} corresponds to the C-C stretching vibrational modes (called ν_{CC}). For determining the detection limit, we choose the most intense Raman peak, which is located at 1072 cm^{-1} , and a detection limit of 230 nM is achieved for the sensing of 4-mPBA molecules (see Fig. 13 where the blue zone corresponds to the zone of the $3\times$ noise level for the last curve) with a signal-to-noise ratio > 3 . Note that the whole frequency signature of 4-mPBA can be easily traced even for the smallest concentration in Fig. 13 by using principle component analysis (see Ref. [63]). We speculate that 4-mPBA detection limit could be much smaller than 10^{-8} M for the considered SERS substrate. In addition, Fig. 13 displays the Raman spectrum obtained in solution (0.5 M). We observe a couple of Raman peaks of 4-mBPA molecules, but also other Raman peaks corresponding to peaks of ethanol.

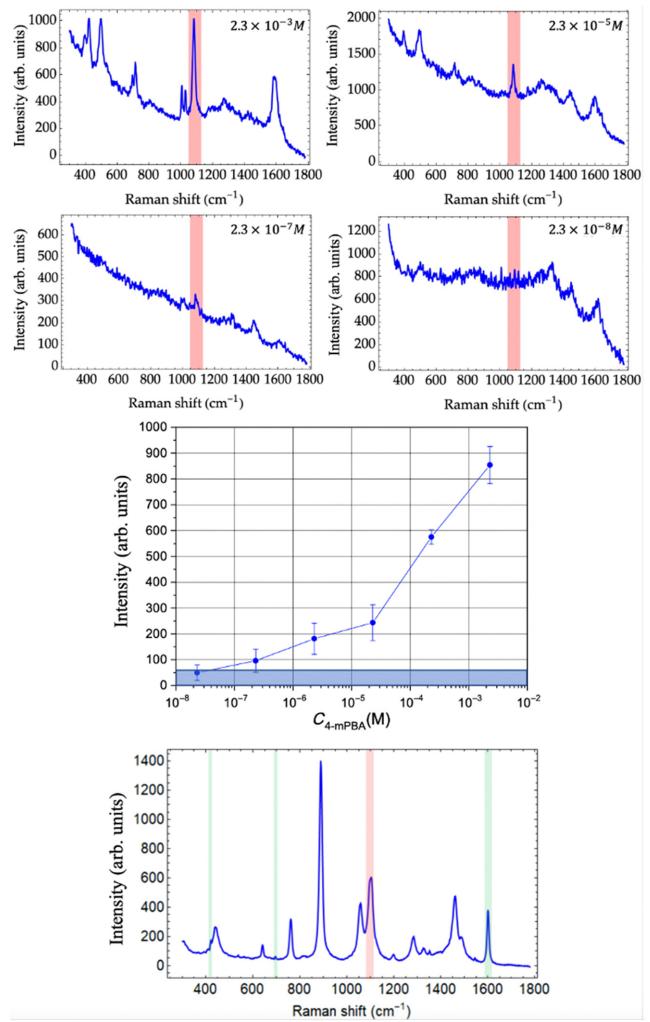


FIG. 13. SERS spectra of 4-mPBA molecules recorded on the metasurface for the concentrations of 2.3×10^{-3} M, 2.3×10^{-5} M, 2.3×10^{-7} M, and 2.3×10^{-8} M, where the red rectangle corresponds to the studied Raman peak. Then, the graph of SERS intensity versus 4-mPBA concentration, where the blue zone corresponds to the zone of the $3\times$ noise level. At the bottom, the Raman spectrum obtained in solution (ethanol) is displayed, where the green and red rectangles correspond to the Raman peaks of the 4-mBPA molecule, and other peaks correspond to ethanol.

We also investigate the spatial distribution of the Raman signal generated by the periodic plasmonic metasurface repeats the morphology of the surface, which is displayed in Fig. 10. Therefore, we can see the SERS effect distributed uniformly over the entire metasurface. The pattern of the Raman signal in Fig. 14 repeats the periodic structure of the modulated film. Therefore, the maxima of the Raman signal repeat the maxima of the plasmon field $I(x, y)$. One could suggest that the SERS is a local effect, namely, $G(x, y) \propto I(x, y)^2$. Investigation of the modulated metal film with progressively smaller period L can confirm the locality of the SERS effect.

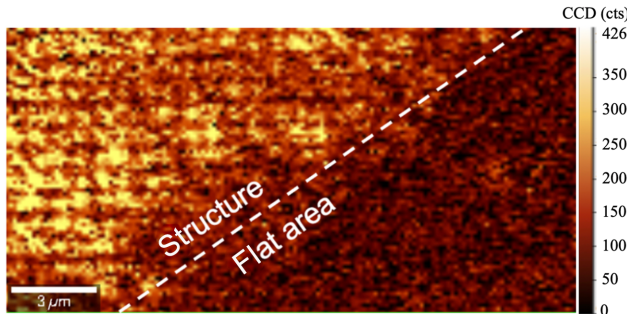


FIG. 14. Optical image of the intensity distribution for the Raman bands 1060–1100 cm^{-1} .

V. CONCLUSIONS

In this paper, we present a study of the low-cost fabrication resonant metasurface consisting of a periodically modulated metal film that exhibits an anomalous optical response due to the excitation of localized surface plasmons. The distribution of the enhanced electric field generated by the film modulation has repeated the surface morphology, and this distribution is uniform over this entire surface. The metal-dielectric metasurface allows a detection limit of 230 nm to be achieved for the 4-mPBA molecules serving here as a proof of concept of SERS sensing. Thus, the low-cost and easy-made SERS metasurfaces modified with 4-mPBA molecules can be used for quantitative biosensing of glycated proteins and sugars. The modulated metal film is the simplest structure formed by holographic lithography technique. We see its advantage in terms of simplicity for mass production. Moreover, nanorod and nanoparticle systems are complementary to the modulated metal film since the nanoparticles and nanorods being deposited on the surface of the film are excited by the local electric field. We can expect the cascade enhancement in the case where size of a metal nanoparticle is much less than the grating period. Moreover, the analytical theory can allow the design and optimization of various plasmonic sensors.

VI. FUNDING

This work is supported by the Russian Foundation for Basic Research (Grant No. 20-21-00080). The Raman measurements are supported by the Russian Science Foundation (Grant No. 21-79-30048).

ACKNOWLEDGMENTS

The authors are grateful to Dr. A.P. Gubarev for important discussions.

[1] B. Sharma, R. R. Frontiera, A.-I. Henry, E. Ringe, and R. P. Van Duyne, SERS: Materials, applications, and the future, *Mater. Today* **15**, 16 (2012).

- [2] J. Yan, X. Han, J. He, L. Kang, B. Zhang, Y. Du, H. Zhao, C. Dong, H. L. Wang, and P. Xu, Highly sensitive surface-enhanced Raman spectroscopy (SERS) platforms based on silver nanostructures fabricated on polyaniline membrane surfaces, *ACS Appl. Mater. Interfaces* **4**, 2752 (2012).
- [3] G. Bodelon, V. Montes-Garcia, V. Lopez-Puente, E. H. Hill, C. Hamon, M. N. Sanz-Ortiz, S. Rodal-Cedeira, C. Costas, S. Celiksoy, I. Perez-Juste, L. Scarabelli, A. La Porta, J. Perez-Juste, I. Pastoriza-Santos, and L. M. Liz-Marzan, Detection and imaging of quorum sensing in *Pseudomonas Aeruginosa* biofilm communities by surface-enhanced resonance Raman scattering, *Nat. Mater.* **15**, 1203 (2016).
- [4] A. K. Sarychev, A. Ivanov, A. Lagarkov, and G. Barbillon, Light concentration by metal-dielectric micro-resonators for SERS sensing, *Materials* **12**, 103 (2019).
- [5] G. Barbillon, A. Ivanov, and A. K. Sarychev, Applications of symmetry breaking in plasmonics, *Symmetry* **12**, 896 (2020).
- [6] J. Henzie, J. Lee, M. H. Lee, W. Hasan, and T. W. Odom, Nanofabrication of plasmonic structures, *Annu. Rev. Phys. Chem.* **60**, 147 (2009).
- [7] Q. Yu, P. Guan, D. Qin, G. Golden, and P. M. Wallace, Inverted size-dependence of surface-enhanced Raman scattering on gold nanohole and nanodisk arrays, *Nano Lett.* **8**, 1923 (2008).
- [8] A.-C. Faure, G. Barbillon, M. Qu, G. Ledoux, O. Tillement, S. Roux, D. Fabreque, A. Descamps, J.-L. Bijeon, C. A Marquette, C. Billotey, C. Jamois, T. Benyatou, and P. Perriat, Core/shell nanoparticles for multiple biological detection with enhanced sensitivity and kinetics, *Nanotechnology* **19**, 485103 (2008).
- [9] V. R. Manfrinato, F. E. Camino, A. Stein, L. H. Zhang, M. Lu, E. A. Stach, and C. T. Black, Patterning si at the 1 nm length scale with aberration-corrected electron-beam lithography: Tuning of plasmonic properties by design, *Adv. Funct. Mater.* **29**, 1903429 (2019).
- [10] G. Barbillon, A. Ivanov, and A. K. Sarychev, SERS amplification in au/si asymmetric dimer array coupled to efficient adsorption of thiophenol molecules, *Nanomaterials* **11**, 1521 (2021).
- [11] P. Zhang, S. Yang, L. Wang, J. Zhao, Z. Zhu, B. Liu, J. Zhong, and X. Sun, Large-scale uniform Au nanodisk arrays fabricated via x-ray interference lithography for reproducible and sensitive SERS substrate, *Nanotechnology* **25**, 245301 (2014).
- [12] G. Barbillon, J.-L. Bijeon, G. Lerondel, J. Plain, and P. Royer, Detection of chemical molecules with integrated plasmonic glass nanotips, *Surf. Sci.* **602**, L119 (2008).
- [13] A. Dhawan, A. Duval, M. Nakkach, G. Barbillon, J. Moreau, M. Canva, and T. Vo-Dinh, Deep UV nano-microstructuring of substrates for surface plasmon resonance imaging, *Nanotechnology* **22**, 165301 (2011).
- [14] N. G. Quilis, M. Lequeux, P. Venugopalan, I. Khan, W. Knoll, S. Boujday, M. L. de la Chapelle, and J. Dostalek, Tunable laser interference lithography preparation of plasmonic nanoparticle arrays tailored for SERS, *Nanoscale* **10**, 10268 (2018).
- [15] J. S. Hwang and M. Yang, Sensitive and reproducible gold SERS sensor based on interference lithography and electrophoretic deposition, *Sensors* **18**, 4076 (2018).

- [16] T. Gong, Y. Luo, C. Zhao, W. Yue, J. Zhang, Y. Zhu, M. Pu, Z. Zuojun, C. Wang, and X. Luo, Highly reproducible and stable surface-enhanced Raman scattering substrates of graphene-Ag nanohole arrays fabricated by sub-diffraction plasmonic lithography, *OSA Continuum* **2**, 582 (2019).
- [17] T. Ding, D. O. Sigle, L. O. Herrmann, D. Wolverson, and J. J. Baumberg, Nanoimprint lithography of Al nanovoids for deep UV SERS, *ACS Appl. Mater. Interfaces* **6**, 17358 (2014).
- [18] C. Farcau, D. Marconi, A. Colnita, I. Brezestean, and L. Barbu-Tudoran, Gold nanopost-shell arrays fabricated by nanoimprint lithography as a flexible plasmonic sensing platform, *Nanomaterials* **9**, 1519 (2019).
- [19] S. Goetz, M. Bauch, T. Dimopoulos, and S. Trassl, Ultrathin sputter-deposited plasmonic silver nanostructures, *Nanoscale Adv.* **2**, 869 (2020).
- [20] J.-F. Masson, K. F. Gibson, and A. Provencher-Girard, Surface-enhanced Raman spectroscopy amplification with film over etched nanospheres, *J. Phys. Chem. C* **114**, 22406 (2010).
- [21] M. Bechelany, P. Brodard, J. Elias, A. Brioude, J. Michler, and L. Philippe, Simple synthetic route for SERS-active gold nanoparticles substrate with controlled shape and organization, *Langmuir* **26**, 14364 (2010).
- [22] G. Barbillon, T. Noblet, B. Busson, A. Tadjeddine, and C. Humbert, Localised detection of thiophenol with gold nanotriangles highly structured as honeycombs by nonlinear sum frequency generation spectroscopy, *J. Mater. Sci.* **53**, 4554 (2018).
- [23] Y. F. C. Chau, K. H. Chen, H. P. Chiang, C. M. Lim, H. J. Huang, C. H. Lai, and N. T. R. N. Kumara, Fabrication and characterization of a metallic dielectric nanorod array by nanosphere lithography for plasmonic sensing application, *Nanomaterials* **9**, 1691 (2019).
- [24] A. I. Kuznetsov, R. Kiyan, and B. N. Chichkov, Laser fabrication of 2d and 3d metalnanoparticle structures and arrays, *Opt. Express* **18**, 21198 (2010).
- [25] G. Barbillon, A. Ivanov, and A. K. Sarychev, Hybrid Au/Si disk-shaped nanoresonators on gold film for amplified SERS chemical sensing, *Nanomaterials* **9**, 1588 (2019).
- [26] A. Lagarkov, I. Boginkaya, I. Bykov, I. Budashov, A. Ivanov, I. Kurochkin, I. Ryzhikov, I. Rodionov, M. Sedova, A. Zverev, and A. K. Sarychev, Light localization and SERS in tip-shaped silicon metasurface, *Opt. Express* **25**, 17021 (2017).
- [27] Q. Zhou, Y. Liu, Y. He, Z. Zhang, and Y. Zhao, The effect of underlayer thin films on the surface-enhanced Raman scattering response of Ag nanorod substrates, *Appl. Phys. Lett.* **97**, 121902 (2010).
- [28] D. Genov, A. K. Sarychev, V. M. Shalaev, and A. Wei, Resonant field enhancements from metal nanoparticle arrays, *Nano Lett.* **4**, 153 (2004).
- [29] K. Seal, A. K. Sarychev, H. Noh, D. A. Genov, A. Yamilov, V. M. Shalaev, Z. C. Ying, and H. Cao, Near-Field Intensity Correlations in Semicontinuous Metal-Dielectric Films, *Phys. Rev. Lett.* **94**, 226101 (2005).
- [30] A. Ivanov, A. Shalygin, V. Lebedev, V. Vorobev, S. Vergiles, and A. K. Sarychev, Plasmonic extraordinary transmittance in array of metal nanorods, *Appl. Phys. A* **107**, 17 (2012).
- [31] L. L. Frumin, A. V. Nemykin, S. V. Perminov, and D. A. Shapiro, Plasmons excited by an evanescent wave in a periodic array of nanowires, *J. Opt.* **15**, 085002 (2013).
- [32] Z.-Q. Liu, G.-Q. Liu, X.-S. Liu, K. Huang, Y.-H. Chen, Y. Hu, and G.-L. Fu, Tunable plasmon-induced transparency of double continuous metal films sandwiched with a plasmonic array, *Plasmonics* **8**, 1285 (2013).
- [33] G.-Q. Liu, Y. Hu, Z.-Q. Liu, Z.-J. Cai, X.-N. Zhang, Y.-H. Chen, and K. Huang, Multispectral optical enhanced transmission of a continuous metal film coated with a plasmonic core-shell nanoparticle array, *Opt. Commun.* **316**, 111 (2014).
- [34] G.-Q. Liu, Y. Hu, Z.-Q. Liu, Y.-H. Chen, Z.-J. Cai, X.-N. Zhang, and K. Huang, Robust multispectral transparency in continuous metal film structures via multiple near-field plasmon coupling by a finite-difference time-domain method, *Phys. Chem. Chem. Phys.* **16**, 4320 (2014).
- [35] I. L. Rasskazov, V. A. Markel, and S. V. Karpov, Transmission and spectral properties of short optical plasmon waveguides, *Opt. Spectrosc.* **115**, 666 (2013).
- [36] A. K. Sarychev, A. V. Ivanov, and G. Barbillon, Generation of plasmon modes in a supernarrow nanoslit formed by silver surfaces, *Quantum Electron.* **51**, 79 (2021).
- [37] V. V. Klimov and D. V. Guzatov, Strongly localized plasmon oscillations in a cluster of two metallic nanospheres and their influence on spontaneous emission of an atom, *Phys. Rev. B* **75**, 24303 (2007).
- [38] V. Klimov and D. Guzatov, Plasmonic atoms and plasmonic molecules, *Appl. Phys. A* **89**, 305 (2007).
- [39] D. V. Guzatov and V. V. Klimov, Optical properties of a plasmonic nano-antenna: An analytical approach, *New J. Phys.* **13**, 053034 (2011).
- [40] A. Demetriadou, J. M. Hamm, Y. Luo, J. B. Pendry, J. J. Baumberg, and O. Hess, Spatiotemporal dynamics and control of strong coupling in plasmonic nanocavities, *ACS Photonics* **4**, 2410 (2017).
- [41] F. Ding, Y. Yang, R. A. Deshpande, and S. I. Bozhevoiyni, A review of gap-surface plasmon metasurfaces: Fundamentals and applications, *Nanophotonics* **7**, 1129 (2018).
- [42] L. A. Vainshtein, *Open Resonators and Open Waveguides* (Golem Press, Boulder, Colo., USA, 1969).
- [43] A. M. Dykhne, A. K. Sarychev, and V. M. Shalaev, Resonant transmittance through metal films with fabricated and light-induced modulation, *Phys. Rev. B* **67**, 195402 (2003).
- [44] X. Deng, G. B. Braun, S. Liu, P. F. Sciortino Jr., B. Koefer, T. Tombler, and M. Moskovits, Single-order, subwavelength resonant nanograting as a uniformly hot substrate for surface-enhanced Raman spectroscopy, *Nano Lett.* **10**, 1780 (2010).
- [45] A. Lagarkov, I. Budashov, V. Chistyakov, A. Ezhov, A. Fedyanin, A. Ivanov, I. Kurochkin, S. Kosolobov, A. Latyshev, D. Nasimov, I. Ryzhikov, M. Shcherbakov, A. Vaskin, and A. K. Sarychev, SERS-active dielectric metamaterials based on periodic nanostructures, *Opt. Express* **24**, 7133 (2016).
- [46] K. N. Kanipe, P. P. F. Chidester, G. D. Stucky, and M. Moskovits, Large format surface-enhanced Raman spectroscopy substrate optimized for enhancement and uniformity, *ACS Nano* **10**, 7566 (2016).

- [47] J. B. Pendry, D. Schurig, and D. R. Smith, Controlling electromagnetic fields, *Science* **312**, 1780 (2006).
- [48] U. Leonhardt, Optical conformal mapping, *Science* **312**, 1777 (2006).
- [49] M. Kraft, Y. Luo, S. A. Maier, and J. B. Pendry, Designing Plasmonic Gratings with Transformation Optics, *Phys. Rev. X* **5**, 1 (2015).
- [50] P. A. Huidobro, Y. H. Chang, M. Kraft, and J. B. Pendry, Hidden symmetries in plasmonic gratings, *Phys. Rev. B* **95**, 1 (2017).
- [51] J. B. Pendry, P. A. Huidobro, Y. Luo, and E. Galiffi, Compacted dimensions and singular plasmonic surfaces, *Science* **358**, 915 (2017).
- [52] J. B. Pendry, P. A. Huidobro, and K. Ding, Computing one-dimensional metasurfaces, *Phys. Rev. B* **99**, 085408 (2019).
- [53] E. Galiffi, J. B. Pendry, and P. A. Huidobro, Broadband tunable thz absorption with singular graphene metasurfaces, *ACS Nano* **12**, 1006 (2018).
- [54] F. Yang, P. A. Huidobro, and J. B. Pendry, Transformation optics approach to singular metasurfaces, *Phys. Rev. B* **98**, 125409 (2018).
- [55] L. Lu, E. Galiffi, K. Ding, T. Dong, X. Ma, and J. B. Pendry, Plasmon localization assisted by conformal symmetry, *ACS Photonics* **7**, 951 (2020).
- [56] F. Yang, E. Galiffi, P. A. Huidobro, and J. B. Pendry, Nonlocal effects in plasmonic metasurfaces with almost touching surfaces, *Phys. Rev. B* **101**, 075434 (2020).
- [57] F. Yang, P. A. Huidobro, and J. B. Pendry, Electron energy loss spectroscopy of singular plasmonic metasurfaces, *Laser Photonics Rev.* **14**, 2000055 (2020).
- [58] L. Dong, X. Yang, C. Zhang, B. Cerjan, L. Zhou, M. I. Tseng, Y. Zhang, A. Alabastri, P. Nordlander, and N. J. Halas, Nanogapped Au antennas for ultrasensitive surface-enhanced infrared absorption spectroscopy, *Nano Lett.* **17**, 5768 (2017).
- [59] J. Kneipp, Interrogating cells, tissues, and live animales with new generations of surface-enhanced Raman scattering probes and labels, *ACS Nano* **11**, 1136 (2017).
- [60] Y. Hu, H. Cheng, X. Zhao, J. Wu, F. Muhammad, S. Lin, J. He, L. Zhou, C. Zhang, Y. Deng, P. Wang, Z. Zhou, S. Nie, and H. Wei, Surface-enhanced Raman scattering-active gold nanoparticles with enzyme mimicking activities for measuring glucose and lactate in living tissues, *ACS Nano* **11**, 5558 (2017).
- [61] C. Andreou, V. Neuschmelting, D.-F. Tschaharganeh, C.-H. Huang, A. Oseledchyk, P. Iacono, H. Karabeber, R. R. Colen, L. Mannelli, S. W. Lowe, and M. F. Kircher, Imaging of liver tumors using surface-enhanced Raman scattering nanoparticles, *ACS Nano* **10**, 5015 (2016).
- [62] H. Chon, S. Lee, S.-Y. Yoon, E. K. Lee, S.-l. Chang, and J. Choo, SERS-based competitive immunoassay of troponin i and ck-mb markers for early diagnosis of acute myocardial infarction, *Chem. Commun.* **50**, 1058 (2014).
- [63] N. L. Nechaeva, I. A. Boginskaya, A. V. Ivanov, A. K. Sarychev, A. V. Eremenko, I. A. Ryzhikov, A. N. Lagarkov, and I. N. Kurochkin, Multiscale flaked silver SERS-substrate for glycated human albumin biosensing, *Anal. Chim. Acta* **1100**, 250 (2020).
- [64] I. N. Kurochkin, A. V. Eremenko, E. G. Evtushenko, N. L. Nechaeva, N. N. Durmanov, R. R. GulievIlyia, I. A. Ryzhikov, I. A. Boginskaya, A. K. Sarychev, A. V. Ivanov, and A. N. Lagarkov, in *Macro, Micro, and Nano-Biosensors*, edited by M. Rai, A. Reshetilov, Y. Plekhanova, and A. P. Ingle (Springer, 2021) Chap. 5, p. 75.
- [65] P. B. Johnson and R. W. Christy, Optical constants of the noble metals, *Phys. Rev. B* **6**, 4370 (1972).
- [66] L. D. Landau, E. M. Lifshitz, and L. P. Pitaevskii, *Electrodynamics of continuous media*, 2nd ed. (Elsevier in Amsterdam, Boston, Oxford, 1993).
- [67] S. Mariazzi, P. Bettotti, S. Larcheri, L. Toniutti, and R. S. Brusa, High positronium yield and emission into the vacuum from oxidized tunable nanochannels in silicon, *Phys. Rev. B* **81**, 235418 (2010).
- [68] F. Brouers, S. Blacher, A. N. Lagarkov, A. K. Sarychev, P. Gadenne, and V. M. Shalaev, Theory of giant Raman scattering from semicontinuous metal films, *Phys. Rev. B* **55**, 13234 (1997).
- [69] D. Barriet, C. M. Yam, O. E. Shmakova, A. C. Jamison, and T. R. Lee, 4-mercaptophenylboronic acid sams on gold: Comparison with sams derived from thiophenol, 4-mercaptophenol, and 4-mercaptobenzoic acid, *Langmuir* **23**, 8866 (2007).
- [70] H. Su, Y. Wang, Z. Yu, Y. Liu, X. Zhang, X. Wang, H. Sui, C. Sun, and B. Zhao, Surface-enhanced Raman spectroscopy study on the structure changes of 4-Mercaptophenylboronic acid under different ph conditions, *Spectrochim. Acta Part A: Mol. Biomol. Spectrosc.* **185**, 336 (2017).
- [71] F. Sun, T. Bai, L. Zhang, J.-R. Ella-Menye, A. K. Liu, Sijunand Nowinski, S. Jiang, and Q. Yu, Sensitive and fast detection of fructose in complex media via symmetry breaking and signal amplification using surface-enhanced Raman spectroscopy, *Anal. Chem.* **86**, 2387 (2014).